Journal of the Korean Society of Oceanography
Vol. 34, No. 1, pp. 22—35, March 1999

An Analytical Model of Co-oscillating Tide under Frictional Effect in the Yellow Sea

SOK KUH KANG, JONG YUL CHUNG[1], YONG Q. KANG[2] AND SANG-RYONG LEE[3]
Coastal and Harbour Engineering Research Center, Korea Ocean Research and Development Institute, Ansan P.O. Box 29, Seoul 425-600, Korea
[1]*Department of Oceanography and Research Institute of Oceanography, Seoul National University, Seoul 151-742, Korea*
[2]*Department of Oceanography, Bukyung National University, Pusan 608-737, Korea*
[3]*Department of Marine Sciences, Pusan National University, Pusan 609-735, Korea*

The response of the tidal waves to friction effect is investigated in terms of deformation of Kelvin and Poincare modes. The 1st Poincare mode does not exist over the low frequency region less than the critical frequency of omega $\omega<\sqrt{2f}$, with $\gamma/f=0.0$, but the mode comes to exist in the presence of friction. When friction exists and its magnitude increases, the wave number increases, indicating that the wave length of the Poincare mode becomes increasingly short with increasing friction. The damping coefficient gradually increases with increasing friction over the high frequency region, but the trend is reversed over the low frequency region. In case of Kelvin wave the present study substantiates the characters of Kelvin wave examined by Mofjeld (1980) and Lee (1988). Based on the examination of frictional effects on the tidal wave propagation, the co-oscillating tides in the Yellow Sea are examined by considering both the head opening and bottom friction effects. As friction is introduced and increased in addition to partial opening at bay head, the location of the amphidromic point near the Shantung Peninsula moves more southwestward. This southwestward movement of the amphidromic point is increasingly compatible with the observed location of Ogura's or Nishida's tidal chart of the M_2 tide.

INTRODUCTION

Tidal phenomena in the seas adjacent to Korea were investigated using both numerical and analytical methods (Ogura, 1933; Defant, 1960; Nishida, 1980; Choi, 1980, 1990; Kang, 1984; Kang *et al.*, 1991, 1998). The tidal waves passing through the Ryukyu Islands experience deformation at the abrupt depth change from 1000—1500 m to 200 m, and the waves propagating into the Yellow Sea are influenced by shallow depths and lateral land boundaries and the M_2 semi-diurnal tide forms 4 amphidromic points in the Yellow Sea. The tidal chart of the M_2 tide by Ogura (1933) is illustrated in Fig. 1a and tidal chart by Kang *et al.* (1998) in Fig. 1b.

Traditionally, the co-oscillating tides in the strait (or channel) and bay have been analytically studied by many researchers. The reflection of a Kelvin wave in a rotating rectangular bay was first studied by Taylor (1921) who solved the problem without considering any dissipation mechanism. Since then, the problem has been continuously generalized by several authors to explain the dynamics of asymmetry of amphidromic system, in terms of head opening, frictional effect, complexity of geometry and energy absorption at bay head. Godin (1965) extended the study to more complicated geometry, consisting of three rectangular seas of constant depth. Hendershott and Speranza (1971) showed that an asymmetry of amphidromic system in such a bay results from a partial absorption of an incident power flux at the bay head. Brown (1973) showed that an asymmetry of the amphidromic system is possible, provided that the tidal period is shorter than the critical period of the first Poincare' mode. Rienecker and Teubner (1980) studied the modification of Taylor's problem by considering the effect of friction in the analysis. They, however, didn't consider the deformation of Kelvin and Poincare waves under friction. The Taylor problem for a finite channel, with friction and an open boundary condition incorporated, was investigated by Fang *et al.* (1991). In the study the asymmetry of

amphidromic system by mutual effects of both friction and head opening was not examined. Among others the asymmetry of the amphidrome in the south of Shantung Peninsula in the Yellow Sea was investigated by Kang (1984) in terms of a partial penetration of the tidal energy through the opening in the head. The friction effect was not introduced in his study, even though the tidal energy dissipation by bottom friction is also expected to contribute to the asymmetry of the amphidromic system.

As outlined above, both the frictional and head opening effects should be taken into consideration simultaneously, in order to explain the asymmetry of the Yellow Sea more realistically. Therefore, this paper aims at investigating the asymmetry of the amphidromic system of the co-oscillating tidal waves in the Yellow Sea, by considering both the friction and head opening effects simultaneously. We also examine the varying characteristics of tidal waves (especially Poincaré wave) in terms of the dispersion relation for each mode by the friction effect.

GOVERNING EQUATION AND BOUNDARY CONDITIONS

Governing equation and boundary conditions

We consider the linear motion of tidal waves for

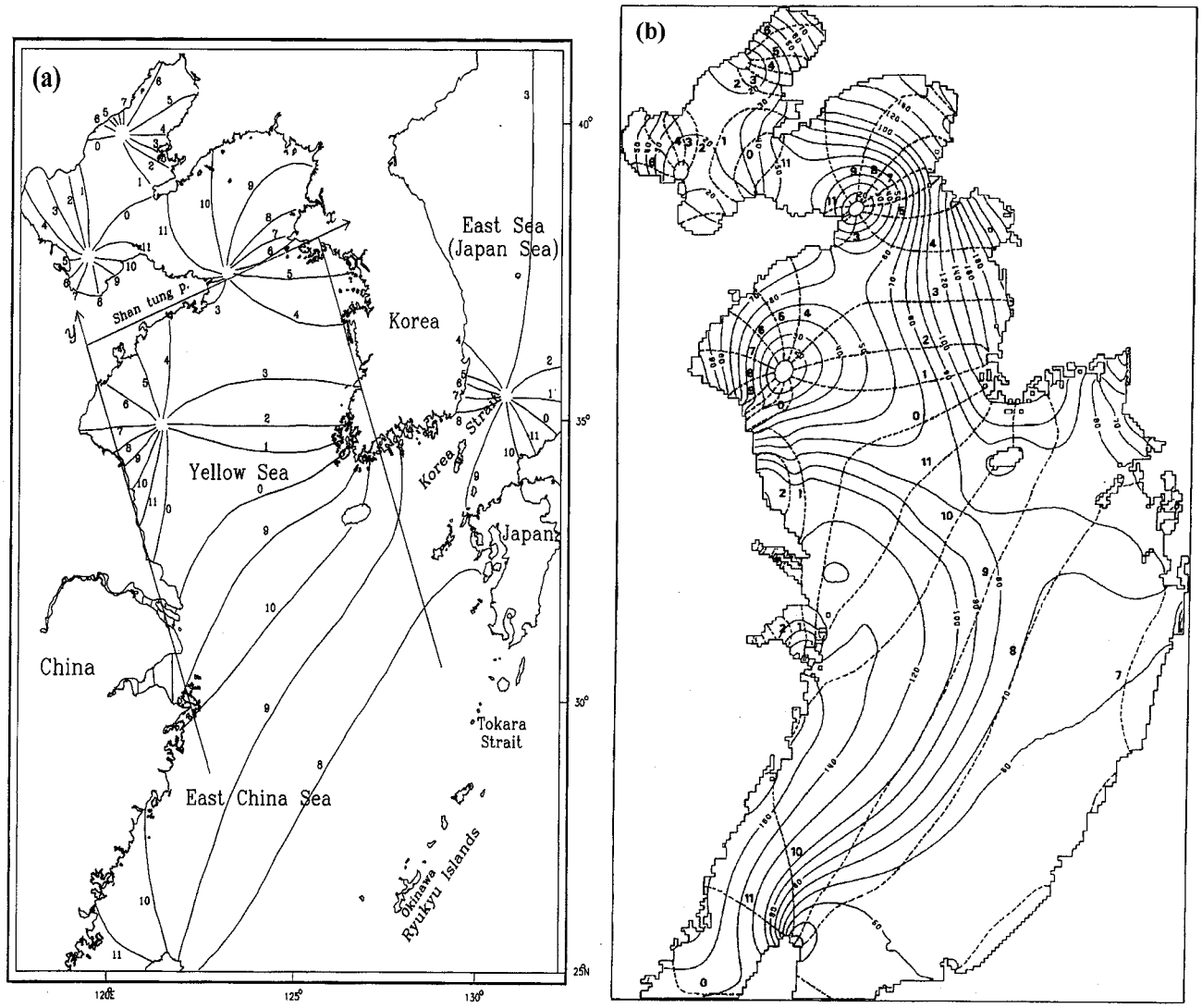

Fig. 1. (**a**) The co-tidal line (lunar hour) of the M_2 tide from Ogura (1933). A rectangular bay of 6 km wide with an open boundary of 200 km long at the head is also presented. (**b**) Computed M_2 tidal chart from Kang *et al.* (1998). Solid line denotes co-amplitude line (cm) and dotted line co-tidal line (lunar hour).

a homogeneous, rotating fluid condition (See Fig.1a for model geometry). The so-called linearized long wave equations (LeBlond and Mysak, 1978) for a homogeneous, rotating fluid with linearized friction can be represented as an alternative form. For the sake of convenience we introduce the linearized mass flux vector by $\vec{U} = iU + jV$, which variables appear after integrating the linearized long wave momentum equations vertically, where

$$U = uH \tag{1a}$$
$$V = vH \tag{1b}$$

with u, v, H being x and y components (Fig. 1a) of particle velocity and water depth, respectively. Then, the integrated long wave equations become

$$\frac{\partial U}{\partial t} = -gH\frac{\partial \eta}{\partial x} + fV - \gamma U \tag{2a}$$
$$\frac{\partial U}{\partial t} = -gH\frac{\partial \eta}{\partial y} + fV - \gamma V \tag{2b}$$
$$\frac{\partial \eta}{\partial t} + \frac{\partial U}{\partial x} + \frac{\partial V}{\partial y} = 0 \tag{2c}$$

where η, g, f, γ denote surface disturbance, gravity acceleration, Coriolis parameter and the linear bottom friction coefficient, respectively. The linearization of quadratic friction is described in Bowden (1983) and also briefly in Kang (1995). Manipulation of the above (2) yields equations in relation to η as follows (see Kang (1995) for details of derivation).

$$\left\{\left(\frac{\partial}{\partial t} + \gamma\right)^2 + f^2\right\}\frac{\partial \eta}{\partial t} = gH\left(\frac{\partial}{\partial t} + \gamma\right)\nabla^2\eta \tag{3a}$$

which is the governing equation for the surface disturbance of tide. Now U and V in terms of η can be derived as follows.

$$\left\{\left(\frac{\partial}{\partial t} + \gamma\right)^2 + f^2\right\}U = -gH\left(\frac{\partial^2}{\partial t \partial x} + f\frac{\partial}{\partial y} + \gamma\frac{\partial}{\partial x}\right)\eta \tag{3b}$$

$$\left\{\left(\frac{\partial}{\partial t} + \gamma\right)^2 + f^2\right\}V = -gH\left(\frac{\partial^2}{\partial t \partial x} - f\frac{\partial}{\partial x} + \gamma\frac{\partial}{\partial y}\right)\eta \tag{3c}$$

The boundary conditions consist of the lateral and head boundary conditions. The lateral boundary condition is that on each of the two lateral walls of the channel the velocity in x-direction must vanish. This condition implies, in view of (3b), that, $U=0$ at $x=0$ and b

$$\left(\frac{\partial^2}{\partial t \partial x} + f\frac{\partial}{\partial y} + \gamma\frac{\partial}{\partial x}\right)\eta = \left(\frac{\partial}{\partial t} + \gamma\right)\frac{\partial \eta}{\partial x} + f\frac{\partial \eta}{\partial y} = 0 \tag{4}$$

Along the open boundary at the bay head we utilize the radiation condition by Proudman (1941) which was used in a rectangular bay with an energy absorbing barrier by Hendershott and Speranza (1971) and also successfully applied to the Yellow Sea by Kang (1984). It is

$$v = \lambda\eta \quad aty = 0 \tag{5}$$

We may use (5) with $\lambda = 0$ along the solid boundary and the following relation is used along the open boundary.

$$\lambda = \delta\frac{\sqrt{gH}}{H} \tag{6}$$

The value δ reflects the rate of tidal energy passing through the opening, and δ is called the radiative factor following Fang *et al.* (1991). The original form of the radiation condition by Proudman (1941) implies that $\delta = 1$. When a partial energy is absorbed in or reflected over the head region, the δ different from 1 may be used.

ANALYTICAL SOLUTIONS

Solution satisfying lateral boundary condition

Let's obtain the solution of (3a) governing η for the lateral boundary condition (4). Wave solutions which are periodic in y and t can be sought in the form

$$\eta = RE\bar{\eta}(x)e^{i(Ly - \omega t)} \tag{7}$$

where L is the wave number in the y direction $\bar{\eta}(x)$ is the (complex) wave amplitude which varies with the cross channel coordinate x. Substitution of (7) into (3a) yields

$$\frac{d^2\bar{\eta}}{dx^2} + \left\{-L^2 - \frac{(-i\omega)(\beta^2 + f^2)}{gH\beta}\right\}\bar{\eta} = 0 \tag{8}$$

where

$$\beta = \gamma - i\omega. \tag{9}$$

Also substitution of (7) into (4) yields

$$\frac{d\bar{\eta}}{dx} + \frac{fiL}{\beta}\bar{\eta} = 0 \tag{10}$$

which is satisfied on $x=0$, b. The general solution of (8) is

$$\bar{\eta}=A\sin\alpha' x+B\cos\alpha' x \tag{11}$$

where

$$\alpha'^2=-\frac{(-i\omega)(\beta^2+f^2)}{gH\beta}-L^2 \tag{12}$$

With substitution of (11) into (10), for two resultant equations satisfied on $x=0$, b, to have nontrivial solutions for A and B, the coefficient determinant of the equations for A and B must vanish, which yields, after some manipulation

$$\sin\alpha' b\left(\alpha'^2-\frac{f^2L^2}{\beta^2}\right)=\sin\alpha' b\left(\alpha'+\frac{fL}{\beta}\right)\left(\alpha'-\frac{fL}{\beta}\right)=0 \tag{13}$$

There are several choices for (13). Let us consider the choices in turn.

Poincaré mode solution

The equation

$$\sin\alpha' b=0 \tag{14}$$

can be satisfied if α' satisfies

$$\alpha'=n\pi/b\,,\qquad n=1,2,3,\cdots. \tag{15}$$

The general solution (11) (Kang, 1995) can be represented as

$$\bar{\eta}_P=\frac{G_n}{\alpha_n'\beta}\left(fL_n\sin\frac{n\pi}{b}x+\alpha_n'\beta\cos\frac{n\pi}{b}x\right) \tag{16a}$$

where $\alpha_n'=i\frac{n\pi}{b}=i\alpha'$ (16b)

The wave solution of (7), then, express η as follows.

$$\eta=RE\,\bar{\eta}_P(x)\,e^{i(Ly-\omega t)}=RE\,[Z_P(x,y)\,e^{-iomegat}] \tag{17}$$

Then, $Z_P(x, y)$ is expressed as

$$Z_P(x,y)=\frac{G_n e^{iL_n y}}{\alpha_n'\beta}\left(\beta\alpha_n'\cos\frac{n\pi}{b}x+fL_n\sin\frac{n\pi}{b}x\right) \tag{18}$$

where L_n and ω are determined from next dispersion relation

$$-gH\beta L_n^2+(\beta^2+f^2)i\omega-\frac{n^2\pi^2}{b^2}gH\beta=0 \tag{19}$$

Even though Rienecker and Teubner (1980) derived the dispersion, they used the relation only for obtaining analytical solution of co-oscillating tides in closed bay and they didn't examine the general character of the dispersion relation. Therefore, we examine the dispersion relation in some details.

In order to examine the dispersion relation of Poincare mode, let $L_n=RE(L_n)+IM(L_n)i$, where RE denotes real part and IM imaginary part. For this mode to propagate in the mouth of the bay or in the negative y, the solution having the negative real value in (19) should be chosen, or

$$RE(L_n)=\frac{\left[\begin{array}{c}\omega^2(\omega^2+\gamma^2-f^2)-(\gamma^2+\omega^2)gH\frac{n^2\pi^2}{b^2}\\+\{(\omega^2(\omega^2+\gamma^2-f^2)-(\gamma^2+\omega^2)gH\frac{n^2\pi^2}{b^2})^2\\+\omega^2\gamma^2(\omega^2+\gamma^2+f^2)^2\}^{1/2}\end{array}\right]^{1/2}}{2gH(\gamma^2+\omega^2)^{1/2}} \tag{20a}$$

and

$$IM(L_n)=\frac{\left[\begin{array}{c}\omega^2(\omega^2+\gamma^2-f^2)+(\gamma^2+\omega^2)gH\frac{n^2\pi^2}{b^2}\\+\{(\omega^2(\omega^2+\gamma^2-f^2)-(\gamma^2+\omega^2)gH\frac{n^2\pi^2}{b^2})^2\\+\omega^2\gamma^2(\omega^2+\gamma^2+f^2)^2\}^{1/2}\end{array}\right]^{1/2}}{2gH(\gamma^2+\omega^2)^{1/2}} \tag{20b}$$

In contrast to the wave number when friction is absent, this wave number has both the real and imaginary parts. Therefore, the Poincare wave becomes a propagating mode with a decaying factor represented by equation (20b). The nondimensional wave number ($R_d RE(L_1)$) and decaying factor ($R_d IM(L_1)$) are plotted against nondimensional wave number (ω/f) for the 1st Poincare mode in Fig. 2, and in Fig. 3 for the 2nd Poincare mode, for northward (positive direction) and southward (negative direction) propagating modes. The critical frequency ω_c ($=2\pi$/critical period (T_c)) is the frequency with which $L_{n=1}=0.0$ in (19) for $\gamma=0.0$. Fig. 2 shows that the 1st Poincare mode does not exist over the low frequency region less than the critical frequency of $\omega<\sqrt{2f}$, with $\gamma/f=0.0$, but the mode

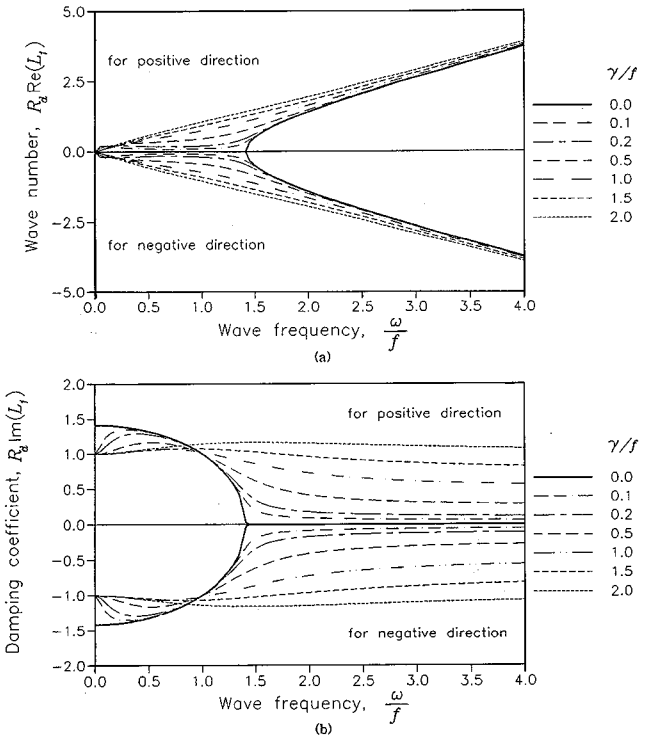

Fig. 2. Wave numbers (**a**) and damping coefficients (**b**) of the 1st Poincare mode (L_1) subject to bottom friction. The wave numbers and damping coefficients, non-dimensionalized by Rossby radius of deformation R_d, are shown against non-dimensional frequency for various values of frictional coefficient (γ/f).

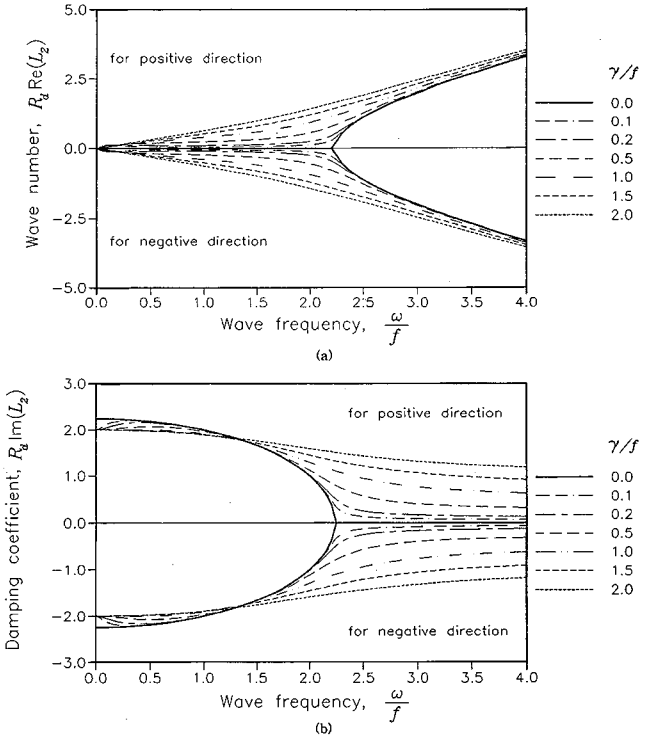

Fig. 3. Wave numbers (**a**) and damping coefficients (**b**) of the 2nd Poincare mode (L_2) subject to bottom friction. The wave numbers and damping coefficient, non-dimensionalized by Rossby radius of deformation R_d, are shown against non-dimensional frequency for various values of frictional coefficient (γ/f).

comes to exist in the presence of friction. Also when $\gamma/f = 0.0$, the mode in the high frequency region over critical frequency propagates without damping. When friction exists and its magnitude increases, the wave number increases. This means that the wave length of the Poincare mode becomes increasingly short with increasing friction. The damping coefficient gradually increases with increasing friction over the high frequency region, but the trend is reversed over the low frequency region. This kind of behavior in wave number and damping coefficient still persists in the 2nd Poincaré mode as shown in Fig. 3. One thing to note is that the magnitude of damping in the 1st Poincaré mode at given frequency is larger than that of the 2nd Poincaré mode, which implies that the 2nd mode decays more rapidly.

Kelvin mode solution

The second case satisfying (13)

$$\alpha'^2 - \frac{f^2 L^2}{\beta^2} = 0 \tag{21a}$$

is divided into two relations, or

$$\alpha' = +\frac{fL}{\beta} \tag{21b}$$

$$\alpha' = -\frac{fL}{\beta} \tag{21c}$$

There exist two solutions satisfying (21a) and (21b), respectively, and superposition of the solutions for the first and second relations yields Kelvin wave solution

$$\bar{\eta}_K(x) = Z_K(x,y) = \eta_o e^{\alpha_i'(x-b)+iL_i y} + \eta_o' e^{\alpha_r' x + iL_r y} \tag{22}$$

where α_i' and α_r' are defined as follows.

$$\alpha_i' = -i\alpha' = -i\frac{fL_i}{\beta_i'} \tag{23a}$$

$$\alpha_r' = -i\alpha' = -i\frac{fL_r}{\beta} \tag{23b}$$

L_i and L_r are solutions of the following dispersion relation

$$\alpha'^2 = \frac{f^2 L^2}{\beta^2} = -(-i\omega)\frac{\beta^2 + f^2}{gH\beta} - L^2 \tag{24}$$

The further mathematical analysis of dispersion relation (24), with $L=RE(L)+IM(L)_i$, is not further attempted, because Mofjeld (1980) studied the characteristics in details and Lee (1988) and Kang (1995) also examined the character of the relation. However, the some aspects of the dispersion, following Kang (1995), are shortly reviewed in order to help to interpret the characteristics of co-oscillating tide in application part later.

Because of the existence of friction, L has an imaginary part. Therefore, the Kelvin wave propagates with damping, as it moves northward or southward. The nondimensional wave numbers ($R_d RE(L)$) and damping coefficients ($R_d IM(L)$) for the northward (positive direction) and southward (negative direction) propagating Kelvin waves are plotted against nondimensional wave number (ω/f) in Fig. 4. The figure shows that the along-channel wave numbers increase, as friction increases. This means that the wave length of the Kelvin waves become increasingly shortened with increasing friction. The damping (decaying) coefficients gradually increase with increasing friction, which implies that as friction increases, the waves decay more rapidly. Note also that when $\gamma=0$, no damping (decaying) occurs.

We proceed to consider the characteristics of α_i' and α_i', which represent the Rossby radius of deformation, when friction exists. (23a) and (23b) can be represented as following form.

$$\alpha_i' = RE(\alpha_i)+IM(\alpha_i)i \text{ and } \alpha_i' = RE(\alpha_i)+IM(\alpha_i)i \tag{25}$$

where α_i' corresponds to the northward or incoming Kelvin mode and α_i' the southward or reflected Kelvin mode, so that the roots satisfying $RE(\alpha_i')>0$ and $RE(\alpha_i')<0$ have been chosen. It is interesting to see that the cross-channel (x) mode comes to have a propagating characteristic only due to the existence of friction, through the existence of a non-zero imaginary part. The real part is an inverse of the Rossby radius of deformation when friction is zero, as shown in (25). The cross-channel non-dimensional wave numbers and damping coeffi-

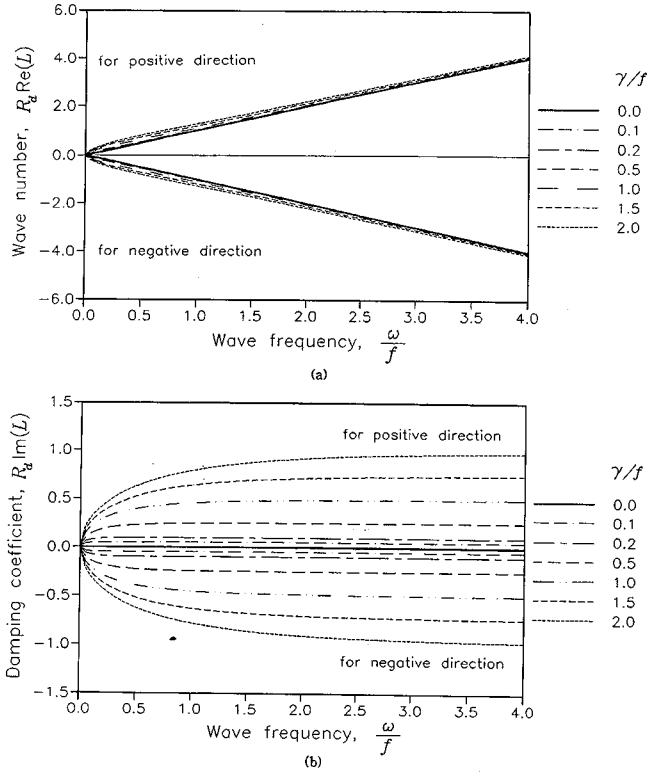

Fig. 4. Along-channel wave numbers (**a**) and damping coefficients (**b**) of the Kelvin waves subject to bottom friction. The wave numbers and damping coefficients, non-dimensionalized by Rossby radius of deformation R_d, are shown against non-dimensional frequency for various values of frictional coefficient (γ/f).

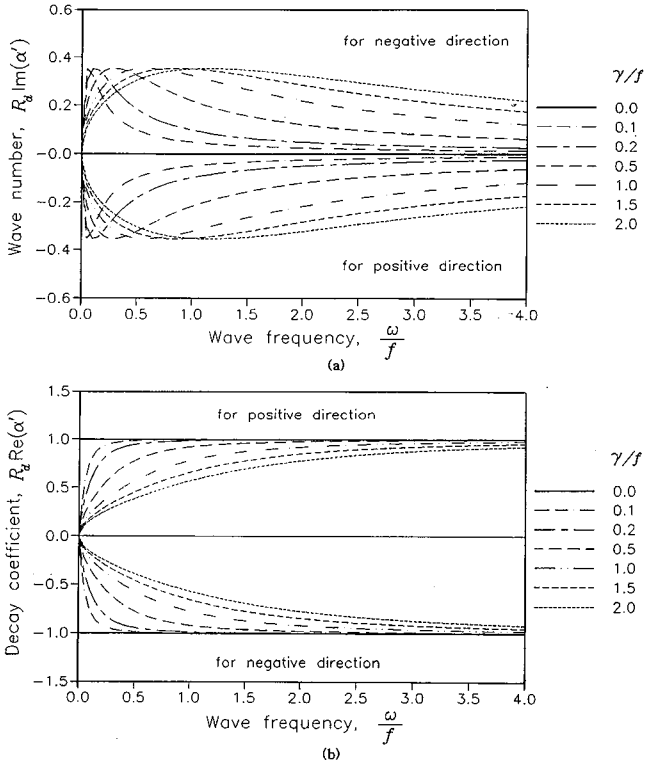

Fig. 5. Cross-channel wave numbers (**a**) and damping coefficients (**b**) of the Kelvin waves subject to bottom friction. The wave numbers and damping coefficients, non-dimensionalized by Rossby radius of deformation Rd, are shown against non-dimensional frequency for various values of frictional coefficient (γ/f).

cients are all shown in Figs. 5a,b for opposingly (eastward and westward) progressing waves. With friction, the deformation radius varies and plays a role as a damping factor for the wave propagating toward the cross-channel; but the magnitudes of the real parts are same for the incoming and reflected waves. This figure shows that the damping coefficients of the cross-channel waves decrease with an increasing friction coefficient, which means that Rossby deformation radius is increased with increasing friction coefficient.

In fact, Mofjeld (1980) pointed out that three important effects of bottom friction on the Kelvin wave propagation existed, which is that 1) the along-channel wavenumber is increased and the offshore or cross-channel wave number is non-zero, 2) the offshore or cross-channel decay increases with an increasing of the wave frequency, and 3) the wave number of the Kelvin wave has no dramatic behavior at the inertial frequency. Lee (1988) made sure of these effects and the results from present study substantiate such characteristics of the Kelvin wave.

Solution satisfying head boundary condition

The solution which satisfies the boundary condition (5) at the head consists of Kelvin and Poincare' waves (LeBlond and Mysak, 1978). A linear superposition of Kelvin waves (22) and Poincare' modes (18) satisfying the boundary condition at the head of bay is

$$Z(x,y)=Z_K+\sum_{n=1}^{\infty} Z_P$$
$$=\eta_o\, e^{\alpha_i'(x-b)+iL_i y}+\eta_o R e^{\alpha_r' x+iL_r y}$$
$$+\sum_{n=1}^{\infty}\frac{G_n e^{iL_n y}}{\alpha_n'\beta}\left(\beta\alpha_n'\cos\frac{n\pi}{b}x+fL_n\sin\frac{n\pi}{b}x\right) \quad (26)$$

where $\eta_o' = \eta_o R$ with R being reflection coefficient.

The boundary condition of (5) at the bay head is used to determine the reflection coefficient of the Kelvin wave and the amplitude of the Poincare' modes. (3c) with $V=RE[\bar{V}e^{-i\omega t}]$ yields

$$(\beta^2+f^2)\bar{V}=-gH\left(\beta\frac{\partial Z}{\partial y}-f\frac{\partial Z}{\partial x}\right) \quad (27)$$

where $Z=Z(x, y)$ is the surface amplitude function and $RE\{\bar{V}e^{-i\omega t}\}$ denote the mass flux in the y direction, with bar $\bar{V}$ being amplitude function of the y mass flux. Using boundary condition (5) with a following form

$$\frac{\bar{V}}{H}=\lambda Z \quad at\ y=0 \quad (28)$$

(27) at the bay head ($y=0$) is

$$(\beta^2+f^2)\bar{V}\,|_{y=0}=-gH\left(\beta\frac{\partial Z}{\partial y}-f\frac{\partial Z}{\partial x}\right)|_{y=0} \quad (29)$$

Then (29) yields, after some manipulation,

$$\sum_{n=1}^{N}G_n\left[\left\{(\beta^2+f^2)\lambda+ig\beta L_n-gf\frac{n\pi}{b}\frac{fL_n}{\alpha_n'\beta}\right\}\cos\frac{n\pi x}{b}\right.$$
$$\left.+\left\{gf\frac{n\pi}{b}+((\beta^2+f^2)\lambda+ig\beta L_n)\frac{fL_n}{\alpha_n'\beta}\right\}\sin\frac{n\pi x}{b}\right]$$
$$+\{(\beta^2+f^2)\lambda+ig\beta L_r-gf\alpha_r'\}A_0 e^{\alpha_r' xR}$$
$$-\{(\beta^2+f^2)\lambda+ig\beta L_i-gf\alpha_i'\}A_0 e^{\alpha_i'(x-b)} \quad (30)$$

where the infinite number of the Poincare' modes are truncated up to the finite mode number N. The reflection coefficient of the Kelvin wave and the amplitude G_n of the Poincare' modes can be determined by the collocation method used by Brown (1973) or the Galerkin technique by Rienecker and Teubner (1980). The equation (30) was solved by the collocation method in this study and matching at (N+1) points is required to get G_n from $n=1$ to N and R. The bay head can be modelled by assigning different values of α according to the configuration of the bay head.

APPLICATION TO CO-OSCILLATING TIDE IN BAY AND IN THE YELLOW SEA

Friction effect on co-oscillating tides in closed bay

We investigate the friction effect on the co-oscillating tide for a bay whose head is completely closed. The bay is assumed to be 600 km wide and 50 m deep, and the Coriolis parameter is evaluated at 36 N. The amplitude of the incident Kelvin wave is assumed to be 1 m. The dimensions of the bay are the same as for the Yellow Sea (Fig. 1a). The periods of the tidal waves are 12.42 and 24 hours,

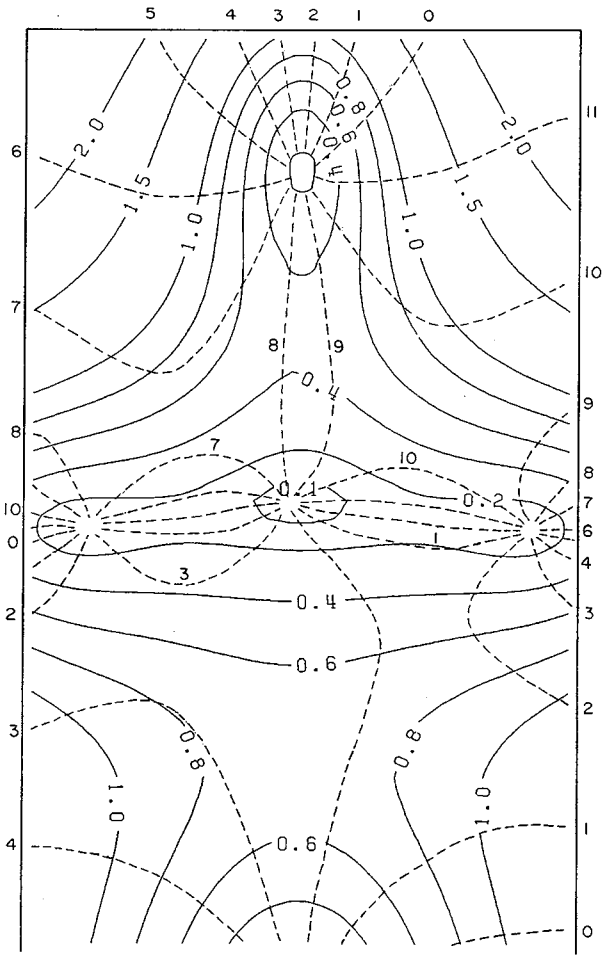

Fig. 6. Tidal chart of the M_2 tide in a rectangular bay of 600 km wide, 1000 km long, and 50 m deep. The result is for friction coefficient $\gamma = 0.0$. Co-tidal line in lunar hours is denoted by dashed line and co-amplitude line in meter is denoted by solid line.

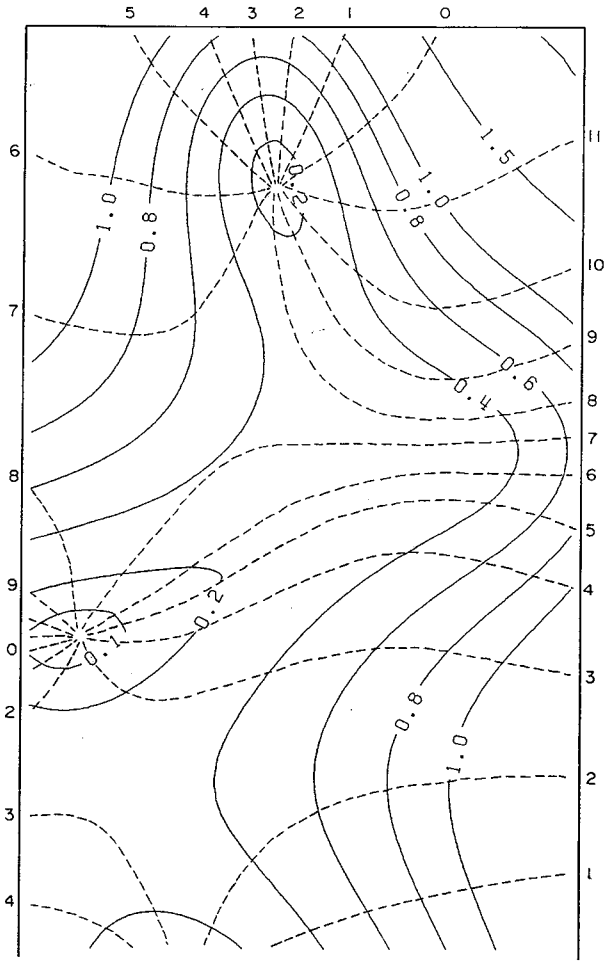

Fig. 7. As in Fig. 6 except for $\gamma = 10^{-5} s^{-1}$.

corresponding to the periods of the M_2 and diurnal tides. The tidal charts in the following figures are obtained by plotting the solutions of (30).

Fig. 6 shows the tidal charts for the M_2 tide in the bay when friction does not exist. The co-amplitude line is denoted by solid lines and the co-tidal lines by dotted lines in the figure. As Kang (1984) computed, the critical period of the first Poincare mode is 12.1 hours. Since the period of the M_2 tide is larger than the critical period, the reflection coefficient $|R| = 1$ and the amphidromic system is almost symmetric. However, the co-amplitude pattern is quite complicated. It is due to the contribution by the Poincare mode whose e-folding distance is 688 km, which is large enough to influence the whole bay of the Yellow Sea. Fig. 7 is the tidal chart for M_2 tide for $\gamma = 10^{-5} s^{-1} (\gamma/f \approx 0.1)$.

It is clear that, as friction is introduced, the symmetry of the amphidromic system disappears. Amphidromic points move toward the wall along which the reflected Kelvin waves propagate. As indicated in Fig. 2, the Poincare mode corresponding to the M_2 frequency propagates along the channel due to the existence of the friction.

As the friction effect is increased (Kang, 1995), the amphidromic point appearing near the center of the bay disappears completely. Also the incoming wave is shown to decay toward the bay head. In other words, due to severe dissipation of the incoming Kelvin wave, the energy of the reflected wave is greatly reduced. Further, the reflected wave is also severely dissipated during the southward propagation. Therefore, the reflected Kelvin wave disappears almost near the mouth of the bay and the solution consists of only an incident Kelvin wave. That is why the amphidromic point almost disappears there. The e-folding distances of Poincare

waves for the band of M_2 tide frequency also become smaller with increasing friction, as indicated in Fig. 2.

The damping coefficients of the Poincare waves for the band of diurnal tides, for the non-dimensional range of friction, less than 1 or so in Fig. 2, are larger than those for the band of semi-diurnal tide. In other words, the e-folding distance of the Poincare mode for the diurnal tide is much less than that for the semi-diurnal tide. Consequently, the amphidromic system of the diurnal tide with $\gamma = 0$ is less complicated than that of the semi-diurnal tide in Fig. 6, because there is less contribution from the Poincare modes. The symmetry of the amphidromic system gradually disappears as friction is introduced and, for $\gamma = 10^{-4} s^{-1}$ (not shown here), the amphidromic point finally lands on the wall along which the reflected Kelvin wave propagates. The damping coefficients of the Kelvin waves over the band of diurnal tides for the relatively large range of friction are less than those for the Kelvin waves over the band of semi-diurnal tides, as shown Fig. 4. This means that, as friction is sufficiently increased, the Kelvin wave in the band of diurnal tide experiences less damping than the Kelvin wave in the higher frequency band.

Head opening effect on co-oscillating tides

Even though some characters of head opening were studied by Kang (1984), the head opening effect is shortly examined as an intermediate step to investigate both the frictional and head opening effects in the bay, since both effects have not been studied simultaneously. The analytical solution is applied to the Yellow Sea with a view to investigating the effects of various head openings. Figs. 8 and 9 are the tidal charts of the M_2 tide for two different head configurations, but the friction effect is not considered in order to clarify the head opening effect. The head of the bay in Fig. 8 consists of a solid boundary of 500 km and open boundary of 100 km. The head of the bay in Fig. 9 consists of a solid boundary of 300 km and an open boundary of 300 km. The λ value in equation (6) is the exact value corresponding to the depth of 50 m, which is less than the value of $\lambda = 0.5 s^{-1}$used by Kang (1984).

The results are as follows: First, as the opening area in the bay head is increased, the contribution by the Poincare mode and reflection coefficient are

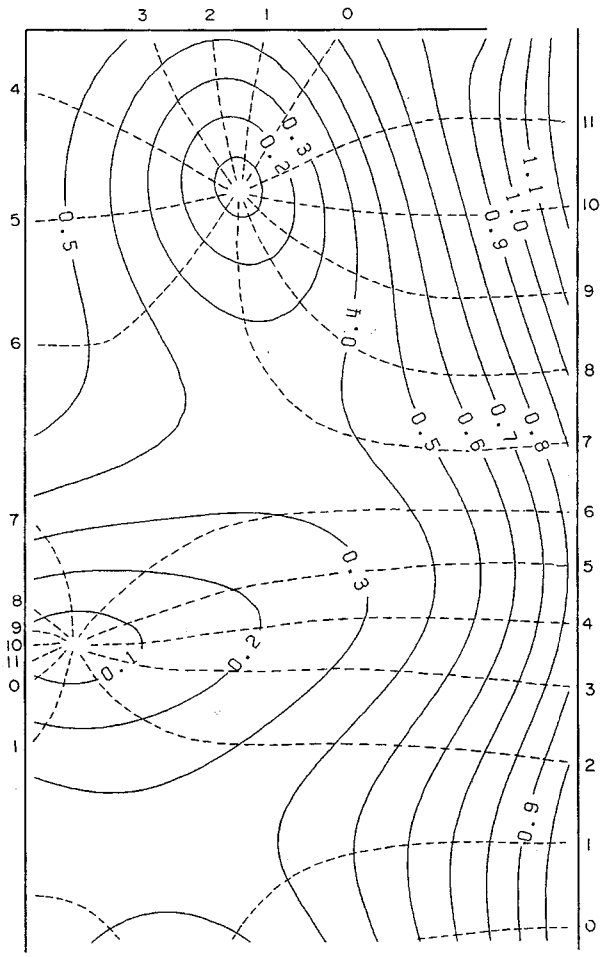

Fig. 8. Tidal chart of the M_2 tide in a rectangular bay with opening at its head. The head configuration consists of a solid boundary of 500 km and an open boundary of 100 km. Other parameters are the same as in Fig. 6.

both decreased (the reflection coefficients for Figs. 8 and 9 are $|R| = 0.303$ and 0.294). In other words, the amplitudes of the Poincare modes and the reflected Kelvin wave are continuously decreased with increasing head opening area, and finally the amplitudes of Poincare modes and reflected Kelvin wave will be zero for the full opening of head. This is due to partial or complete penetration of incident energy flux through the opening. Second, due to the decreasing contribution of the Poincare modes with an increased opening, the solution of the co-oscillating tide consists of mainly opposingly progressing Kelvin modes, even near the head of bay, except for the case of a full opening. Third, as the contribution by the Poincare modes is decreased, the phase lags of reflected Kelvin wave are reduced over the process of reflection. This results in the southward movement of the along-bay position of

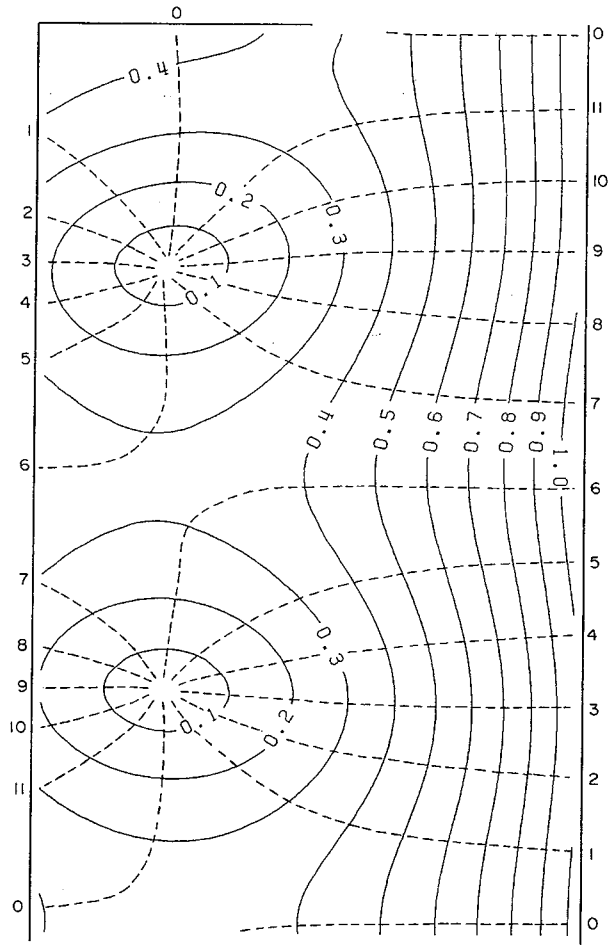

Fig. 9. As in Fig. 8 except for the head configuration of a solid boundary of 300 km and an open boundary of 300 km.

the amphidromic point located at upper site of the bay, to the location which is nearly a quarter of a wave length apart from the head. This fact is manifest when comparing the along-bay locations between Figs. 8 and 9.

In the case of the full opening, the reflection coefficient is equal to zero and the magnitudes of the Poincare modes are nearly zero, which means that the solution consists of only the incident Kelvin wave. The exponential decrease of amplitude toward the wall along which the reflected Kelvin wave propagates and the propagation pattern from the south reflect that there exists only an incident Kelvin wave. This also implies that the radiation condition of Proudman works very well.

For diurnal tide the same trend is also found as that for the M_2 tide (Kang, 1995). However, as mentioned before, the e-folding distance of the Poincare modes in this period are much shorter than that for the M_2 tide and the amplitudes of the Poincare modes are also smaller than those for the M_2 tide.

In summary, the amplitudes of the reflected Kelvin wave and the Poincare modes are gradually decreased with the increased widening of the open boundary at the head. This is due to the partial penetration of incident energy flux, as noted by Kang (1984). Further, as the opening area at the bay head becomes wide, the along-bay location of the amphidromic point of the M_2 tide existing near the bay head, moves southward to the position approximately a quarter of a wavelength apart from the head. Also, with increased widening of head opening, the cross-bay locations of the two amphidromic points of the M_2 tide nearly coincide with each other, until they land on the wall along which the reflected Kelvin wave travels. This is due to the decreased contribution of Poincare modes even near the head, since e-folding distance is largely reduced.

APPLICATIONS TO CO-OSCILLATING TIDES IN THE YELLOW SEA

In this section the friction effect along with head opening effect is investigated for the more realistic understanding of the tidal system in the Yellow Sea. The bottom friction is especially expected to play a meaningful role in the amphidromic system due to the shallowness of the Yellow Sea.

The dimensions of the bay are the same as in previous section, but the head configuration consists of a solid boundary of 300 km, an open boundary of 200 km and another solid boundary of 100 km, as schematized in Fig. 1a, which shows the tidal chart of the M_2 tide edited by Ogura (1933). The location of the amphidromic point located below Shantung Peninsula agree with those of the results of the numerical model done previously by Choi (1980) and Kang *et al.* (1998). As shown in previous part the character of co-oscillating tides in the Yellow Sea is largely governed by the magnitude of the friction coefficient. Therefore, the proper choice of the friction coefficient is important and the theoretical background for choosing it should be explained. Before discussing the properness of chosen friction coefficient (γ), the co-oscillating tide is investigated for $\gamma = 0.0, 5.010^{-6}$, $1.0 \times 10^{-5}, 2.5 \times 10^{-5} s^{-1}$. Practically when the mean speed of M_2 tidal current in Yellow Sea is assumed

to be 0.5 m/s, the friction coefficient following Kang (1995) is $2.5\times 10^{-5}s^{-1}$.

If the damping effect caused by other components are introduced, the magnitude of the friction coefficient will be slightly increased, since the damping effect for M_2 is mostly dependent upon the magnitude of itself, as investigated by Godin and Gutierrez (1986).

Figs. 10 and 11 show the tidal charts of the M_2 tide for the friction coefficient $\gamma= 0.0,2.5\times 10^{-5}s^{-1}$. The reflection coefficients of the Kelvin wave for the figures are $|R|=0.163$ and 0.212, respectively, and the phase shifts of the reflected Kelvin wave are decreased from 86° to 29°, respectively. As friction is increased, the amplitudes of Poincare modes are decreased and e-folding distances of the 1st Poincare mode are also gradually decreased from 688 km to 416 km.

The figures show that as friction is increased, the locations of the amphidromic points move southwestward from 225—155 km of Fig. 10, to 145—185 km of Fig. 11. This southwestward movement of the amphidromic point is increasingly compatible with the location 135—220 km of Ogura's tidal chart of the M_2 tide found in Fig. 1a. That is, the friction effect is shown to be necessary in explaining the actual amphidromic system of the M_2 tide more realistically, as expected. One point to note is that the distance of westward movement of the amphidrome by bottom friction ($\gamma= 2.5\times 10^{-5}$ s^{-1}) is almost the same as that by head opening effect at an approximate 75 km.

It is also interesting to note that comparing Fig. 10 with Figs. 8 and 9, the amphidromic point located at the lower part of bay has disappeared and the along-bay location 225—155 km of the existing amphidromic point is closer to the bay head than the previous location 235—180 km of Fig. 8. Con-

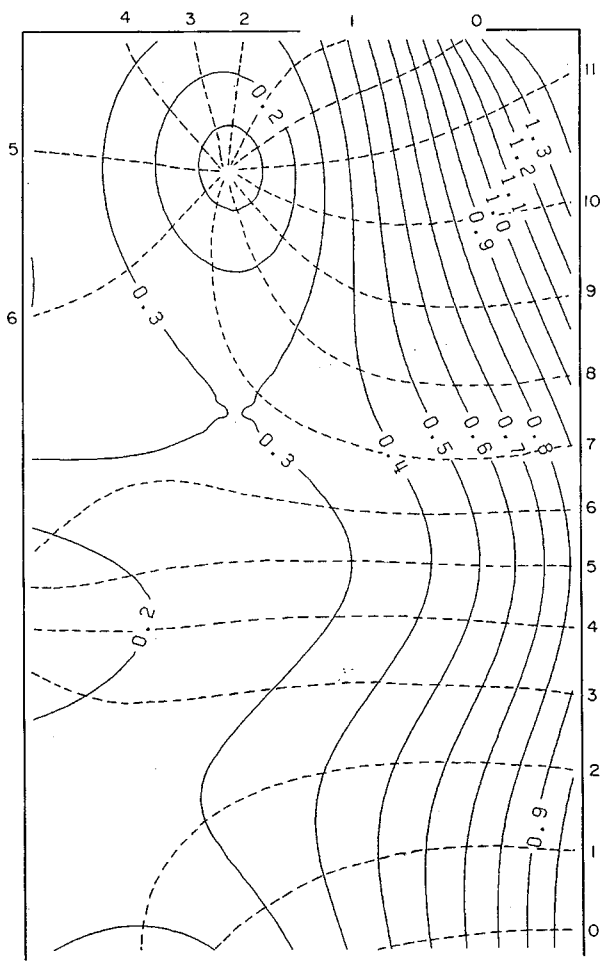

Fig. 10. As in Fig. 3.11 except for the head configuration of an open boundary of 600 km.

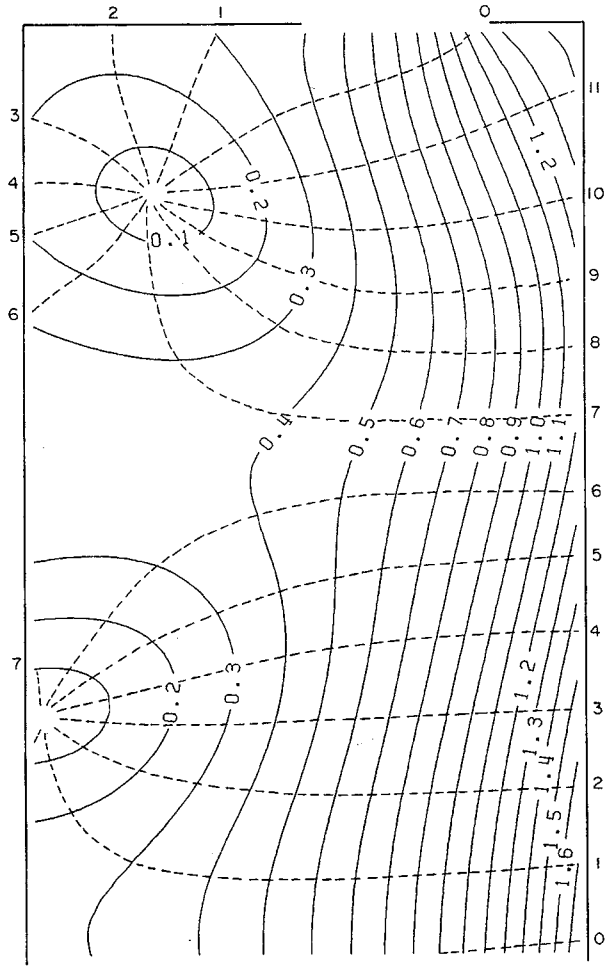

Fig. 11. Tidal chart of the M_2 tide subject to partial opening of bay head and bottom friction $\gamma= 2.5\times 10^{-5}s^{-1}$.

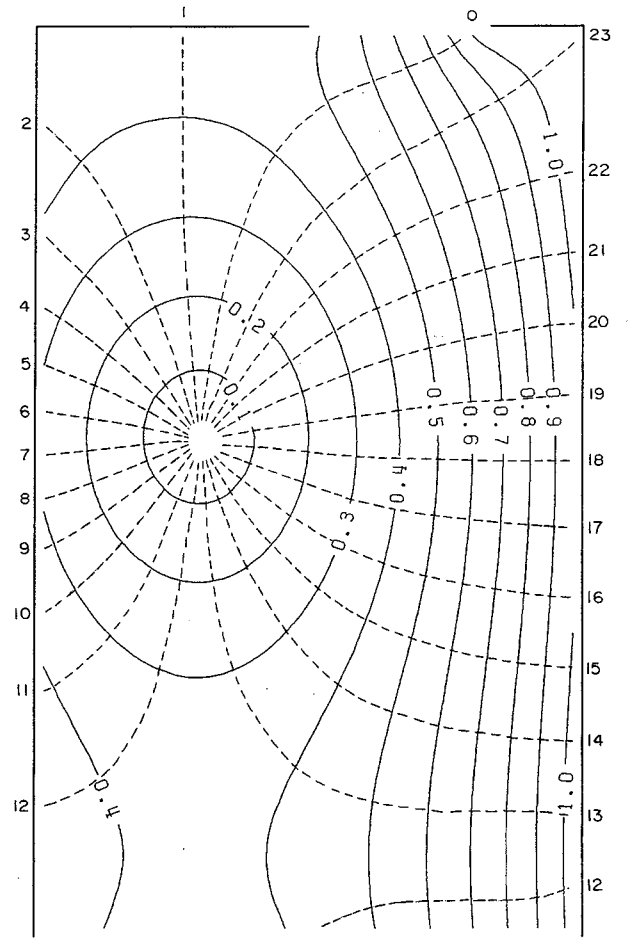

Fig. 12. Tidal chart of the diurnal-tide with a period of 24 hrs subject to partial opening of bay head and bottom friction $\gamma = 0.0$.

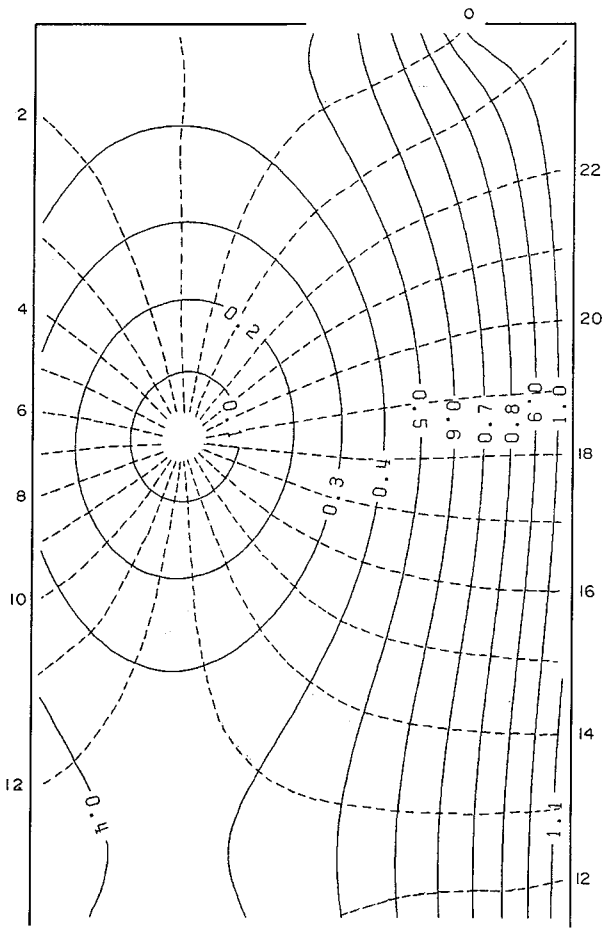

Fig. 13. As in Fig. 12 except for $\gamma = 5 \times 10^{-6} s^{-1}$.

sidering that the location of the upper amphidromic point moves southward with an increasingly widening of the head, the Poincare mode still appears to be influential in respect to the tidal system in bay. As a result, the phase shift of the reflected Kelvin wave is still as large as 86° (note that the phase shift $= 127°$ with no open boundary in Fig. 6). Also the amphidromic point located in the lower part shows up more clearly with increasing friction.

Figs. 12, 13, 14 and 15 are the tidal charts of the diurnal tide for $\gamma = 0.0$, 5×10^{-6}, 10^{-5}, 2.5×10^{-5} s^{-1}, respectively. Considering the tidal range of the diurnal tide and M_2 tide and assuming that the speed of the current is proportional to the tidal ranges, the speed of the diurnal current is about 0.3 times as large as that of the M_2 tidal current. Therefore, when the speed of the diurnal tide in the Yellow Sea is assumed to be 0.1 m/s, the friction coefficient is

$$\gamma = \frac{K_b}{H} |u| = \frac{0.0025}{50} 0.1 = 5 \times 10^{-6} s^{-1}.$$

As shown in Kang (1995), the diurnal component with lesser amplitude undergoes more severe dissipation by other semi-diurnal components with larger amplitude. Therefore, the coefficient of friction is increased 2 or 3 times larger than the coefficient without interaction.

The reflection coefficients of the Kelvin wave for the figures shown above are $|R| = 0.118$ and 0.120, and the phase shifts of reflected Kelvin wave are 14° and 13°. As friction coefficient is increased from 0.0 to 2.5×10^{-5} s^{-1}, the amplitudes of Poincare modes increase slightly from 0.118 to 0.133 while the e-folding distances of the 1st Poincare mode change from 178 km to 181 km. This small change according to the varying friction has been shown around diurnal tide frequency($\omega/f = 0.85$) in the Fig. 2b. Compared with the amplitudes and e-folding distances in the M_2, the role played by Poincare

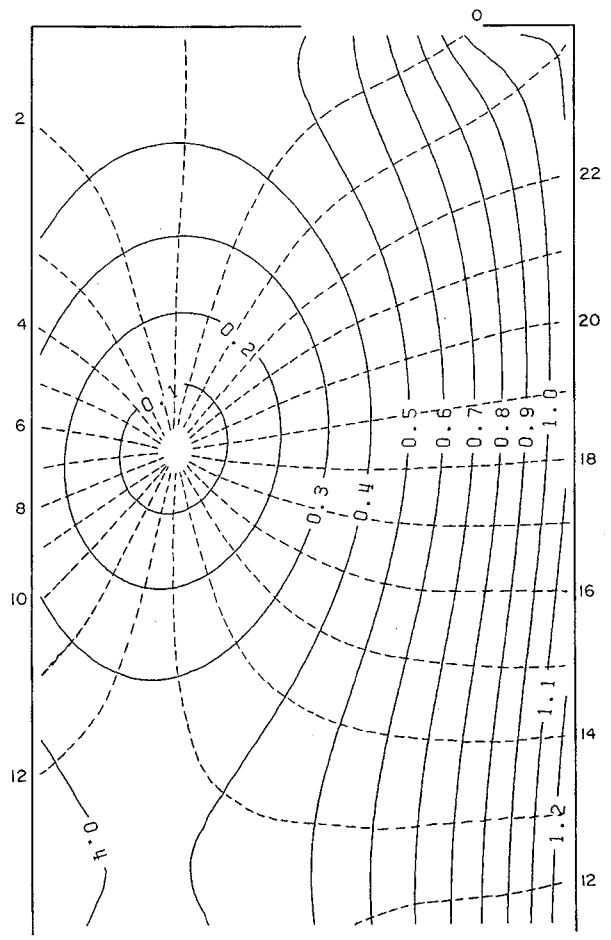

Fig. 14. As in Fig. 12 except for $\gamma = 10^{-5} s^{-1}$.

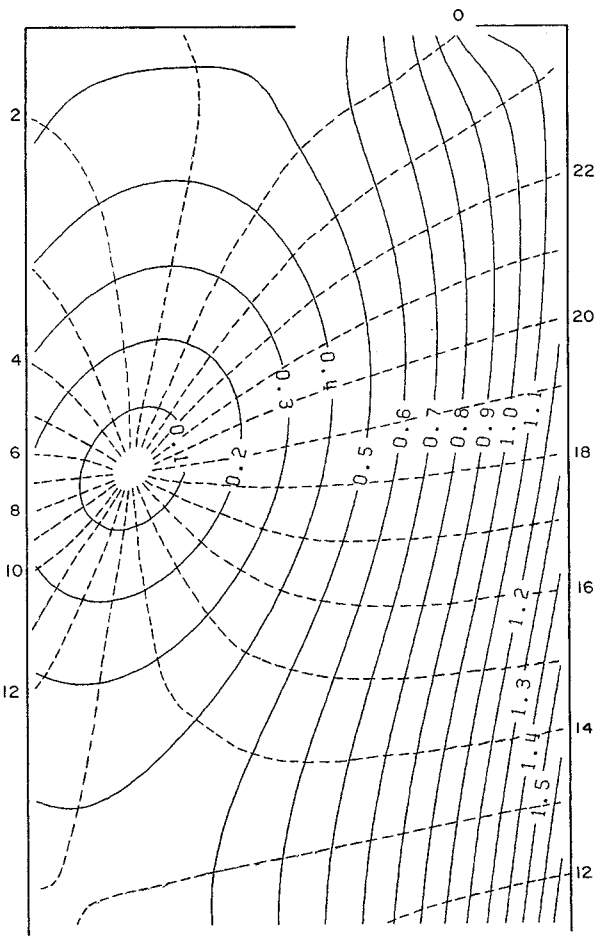

Fig. 15. As in Fig. 12 except for $\gamma = 2.5 \times 10^{-5} s^{-1}$.

modes is expected to be small in determining the position of the amphidromic point.

The figures illustrate that with increasing friction ($\gamma = 0.0$, 5×10^{-6}, 10^{-5}, 2.5×10^{-5} s^{-1}) the amphidromic points move slightly southwestward. The locations of amphidromic points are 185—460 km, 175—465 km, 160—470 km, and 120—490 km, respectively. The location of the amphidromic point from the numerical model and Ogura's tidal chart for K_1 is approximately 230—300 km. The aforementioned amphidromic point is located more eastward than that of the M_2 tide. It is evident that the inconsistency for the locations between the analytical model and the available diurnal tidal chart increases with increasing friction. In fact, the magnitude of the friction coefficient (γ) is much smaller than that of the M_2 tide, as shown above. This implies that the diurnal tide is less dissipated due to its reduced magnitude of current speed.

Considering that the e-folding distances of the 1st Poincare mode are less than 200 km and their amplitudes are relatively small, such a movement must be explained mainly in terms of Kelvin waves. The southward movement seems to be driven by a decreased phase shift of the reflected Kelvin wave while the westward movement is expected to be due to the decreased amplitude of the reflected Kelvin wave by friction toward the southward direction.

It should be mentioned that the nonuniformity of the bottom topography will also distort the tidal regime in the Yellow Sea. In particular the shallowness near the Yangtze river would induce a locally severe dissipation of the tidal wave, while the irregular coastal line near the river would also influence the propagation of tidal wave. These effects could not be taken into consideration due to the limitations of the present model.

SUMMARY

The bottom frictional effect to the tidal waves in the Yellow Sea have been studied along with the

head opening effect. In addition to head opening as friction is introduced and increased, the location of the amphidromic point near Shantung Peninsula moves southwestward. This southwestward movement of the amphidromic point is increasingly compatible with the observed location of Ogura's tidal chart of the M_2 tide, implying that the inclusion of the friction effect is necessary to explain the actual amphidromic system of the M_2 tide more realistically. The results show that the distance of the westward movement of amphidrome by bottom friction ($\gamma = 2.5 \times 10^{-5} s^{-1}$) is almost the same as that by the head opening effect at an approximate 75 km. It was also found that the westward movement of amphidromic point near the head with increasing friction is caused by the increased dissipation and decreased e-folding distance of the Poincare modes. The southward movement of the amphidromic point is driven by both the decrease of phase shift of the reflected Kelvin wave and the decreasing role of the Poincaré mode, with increasing friction effects.

The dispersion relation of tidal waves have been examined under friction effect. The 1st Poincaré mode does not exist over the low frequency region less than the critical frequency of $\omega < \sqrt{2f}$, with $\gamma/f = 0.0$, but the mode comes to exist in the presence of friction. When friction exists and its magnitude increases, the wave number increases, indicating that the wave length of the Poincaré mode becomes increasingly short with increasing friction. The damping coefficient gradually increases with increasing friction over the high frequency region, but the trend is reversed over the low frequency region. This kind of behavior in wave number and damping coefficient still persists in the 2nd Poincaré mode. The magnitude of damping in the 1st Poincaré mode at given frequency is larger than that of the 2nd Poincare' mode. In case of Kelvin wave the present study substantiate the characters of the Kelvin wave examined by Mofjeld (1980) and Lee (1988).

ACKNOWLEDGMENTS

We thank two reviewers for their valuable comments and suggestion on the earier draft of this manuscript.

REFERENCES

Bowden, K.F., 1983. Physical Oceanography of Coastal Waters. Ellis Horwood Ltd., Chichester, 298 pp.

Brown, P.J., 1973. Kelvin-wave reflection in a semi-infinite canal. *J. Mar. Res.*, **31**: 1–10.

Choi, B.H., 1980. A Tidal Model of Yellow Sea and Eastern China Sea. KORDI Report, 80–02, Korea Ocean Research and Development Institute, Seoul, 72 pp.

Choi, B.H., 1990. Development of fine-grid numerical tidal models of the Yellow Sea and the East China Sea. *J. Korean Soc. Coast. Ocean Eng.*, **2**: 231–234.

Defant, A., 1960. Physical Oceanography, Volume II, Pergamon Press, Oxford, 598 pp.

Fang, Z., A. Ye and G. Fang, 1991. Solutions of tidal motions in a semi-closed rectangular gulf with open boundary condition specified. In: Tidal Hydrodynamics, edited by Parker, B., John Wiley & Sons Inc., New York, pp. 153–168.

Godin, G., 1965. The M_2 tide in the Labrador Sea, Davis Strait and Baffin Bay. *Deep-Sea Res.*, **12**: 469–477.

Godin, G., 1991. Compact approximation to the bottom friction term, for the study of tides propagating in channels. *Cont. Shelf Res.*, **11**: 579–589.

Hendershott, M.C. and A. Speranza, 1971. Co-oscillating tides in long narrow bays: the Taylor problem revisited. *Deep-Sea Res.*, **18**: 959–980.

Kang, S.K., S.R. Lee, K.D. Yum, 1991. Tidal computation of the East China Sea, the Yellow Sea and the East Sea. In: Oceanography of Asian Marginal Seas, edited by K. Takano, *Elsevier Oceanography Series* 54, Amsterdam, pp. 25–48.

Kang, S.K., 1995. An Analytical Model of Tidal Waves in Bay and Strait under Current Effect. Ph.D. Thesis, Seoul National University, Seoul, 173 pp.

Kang, S.K., S.R. Lee and H.J. Lee, 1998. Fine grid tidal modeling of the Yellow and East China Seas. *Cont. Shelf Res.*, **18**: 739–772.

Kang, Y.Q., 1984. An analytical model of tidal waves in the Yellow Sea. *J. Mar. Res.*, **42**: 473–483.

LeBlond, P.H. and L.A. Mysak, 1978. Waves in the Ocean. Elsevier Scientific Publishing Company, Norwich, 602 pp.

Lee, S.H., 1988. Scattering of the Tidal Waves and Residual Currents around an Island on the Shelf Sea. Ph.D. Thesis, Seoul National University, Seoul, 236 pp.

Mofjeld, H.O., 1980. Effects of vertical viscosity on Kelvin waves. *J. Phys. Oceanogr.*, **10**: 1039–1050.

Nishida, H., 1980. Improved tidal charts for the western part of the north Pacific Ocean. *Rept. Hydrogra. Res.*, **15**: 55–70.

Ogura, S., 1933. The tides in the Seas adjacent to Japan. *Hydrogra. Bull. Dep. Imp. Jap. Navy*, **7**: 1–189.

Pedlosky, J., 1987. Geophysical Fluid Dynamics (2nd ed.), Springer-Verlag, Virginia, 710 pp.

Proudman, J., 1941. The effects of coastal friction on the tides. *Mon. Not. R. Astr. Soc. Geophys. Suppl.*, **5**: 23–26.

Rienecker, M.M. and M.D. Teubner, 1980. A note on frictional effects in Taylor's problem. *J. Mar. Res.*, **38**: 183–191.

Taylor, G.I., 1921. Tidal oscillation in gulfs and rectangular basins. *Proc. Lond. Math. Sec.*, **33**: 148–181.

Manuscript received November 9, 1998
Revision accepted January 28, 1999